Numerical Study on the Performance Characteristics and Pressure Pulsation of the Electric Scroll Compressor

Kai Ma[1], Zhilong He[1]*, Dantong Li[1], Minglong Zhou[2], Wenqing Chen[2]

[1]Xi'an Jiaotong University, School of Energy and Power Engineering,
Xi'an, Shaan Xi, China
(monkey8023@stu.xjtu.edu.cn)

[2] Xi'an Jiaotong University, Suzhou Academy,
Suzhou, Jiang Su, China

* Corresponding Author
zlhe@mail.xjtu.edu.cn

ABSTRACT

Scroll compressors were widely employed in electric vehicles due to their high efficiency, low noise, and low vibration. The electric scroll compressor is operated through direct motor drive, with motor cooling facilitated by the intake refrigerant. After compression, the refrigerants were exhausted through the oil and gas separation structure. However, substantial pressure loss occurs due to the larger intake and exhaust flow areas compared to the scroll area. This paper presents a complete computational fluid dynamics (CFD) model of the electric scroll compressor. The model incorporates domains for the motor, the rotating main balance weight, the crescent-shaped scroll compression chambers, as well as the exhaust buffer chamber and oil separator. Through calculations, the pressure and temperature distribution within the scroll compressor are determined. Under specified operating conditions, as the rotational speed escalates from 5000 rpm to 10000 rpm, the inlet pressure loss experiences an increment from 5-15 kPa to 25-55 kPa. Concurrently, the exhaust fluctuation transitions from 15-15.9 bar to 16-17.8 bar. Comparatively, the simplified model exhibits significantly enhanced volumetric efficiency and isentropic efficiency. When simplifying the model and establishing boundaries, the pressure loss should be considered on the operating conditions to enhance calculation accuracy. The developed complete CFD model serves as a valuable tool for analyzing and enhancing the performance of electric scroll compressors.

1. INTRODUCTION

Electric scroll compressors are widely employed in electric vehicle air conditioner system due to their advantages of high energy efficiency, low vibration, and low noise. Typically, scroll compressors designed for electric vehicles utilize lightweight aluminum alloy materials to ensure compactness and weight savings. These compressors are directly driven by motors and are often configured horizontally to optimize installation space. Currently, electric scroll compressors are mainly used in fields such as electric buses and passenger cars. Variable frequency motors are frequently utilized to adjust the speed of electric scroll compressors, allowing them to meet the demands of various operating conditions. At present, most scroll compressors for electric vehicles on the market use PMP profiles. In order to increase the suction volume and improve the compressor, researchers use variable thickness profiles and variable tooth height structures. Additionally, steam injection is being investigated to improve scroll compressor performance (Zhang et al., 2022).

The profile of the scroll compressor can be involute, variable base circle radius involute, algebraic spiral, etc. Considering the processing factors, arcs, arc straight lines, etc. are used to modify the profile at the beginning (Zhang et al., 2024). Peng (Peng et al., 2017) use circular involutes, advanced curves and arcs to form the scroll profile. They use double arc correction at the profile beginning to establish a thermodynamic model, achieving an experimental prototype with an error of less than 5% in comparison to the experimental data. Zhang (Zhang et al.,

2023) developed a general method for generating variable wall thickness profiles. They successfully designed a scroll compressor with a displacement of 34mL. While its performance closely resembled that of a compressor with a fixed wall thickness, the wrap height of the variable wall thickness model was 5.8% smaller, with an increased thickness at the beginning of the scroll center.

Variable scroll wrap height can be divided into two types: stepped variable warp height and gradual variable wrap height. In the stepped variable wrap height design, the wrap height at the suction end is set higher than that in the compression chamber. In the gradual variable wrap height design, the wrap height gradually decreases from the suction to the exhaust. TAKASU et al. (TAKASU et al., 2019) developed scroll compressors with variable wrap height, referred to 3D scroll and e-3D scroll respectively. Under rated load conditions, the efficiency of both type is comparable. However, at 50% and 25% load, the efficiency is increased by 3.2% and 4.8% respectively. Particularly under low-speed operating conditions, e-3D can reduce leakage losses and improve energy efficiency.

Research on scroll compressor performance mainly uses theoretical chamber models, computational fluid dynamics (CFD) models and experimental analysis. While theoretical calculations and experimental analysis provide the overall performance of the compressor, they cannot predict the unsteady flow of the working fluid in the chamber. Through CFD simulation, the pressure and temperature inside the scroll can be obtained, and its internal flow conditions can be analyzed to provide a basis for optimization. Cavazzini et al. (Cavazzini et al., 2021) observed unsteady flow within the scroll chamber during suction and exhaust processes. They noted that axial gap leakage reduces compressor volume and increases power consumption. The asymmetric suction chamber of the scroll compressor introduces parameter asymmetry and vortex flow asymmetry, leading to increased exhaust resistance loss (Sun et al., 2017; Ding et al., 2022). Sun et al. (Sun et al., 2019,2021) studied the structure of the suction passage and the OS head of the scroll compressor using the CFD method. They found that the suction passage of the shrinking scroll compressor can effectively improve the volumetric efficiency, but may increase the flow pulsation. Additionally, to avoid the impact of the asymmetry of the scroll chamber on the exhaust pulsation, an optimization algorithm is employed to determine the optimal correction angle of the OS head. The optimization resulted in a 4.11% increase in volumetric efficiency, a 4.91% increase in isentropic efficiency, and effectively reduced of exhaust losses.

As the rotating speed increases, the pressure fluctuations within the compression chamber and exhaust process intensify, leading to over-compression. Additionally, the maximum axial and tangential leakage occurs at the center of the scroll in the compression chamber (Li et al., 2023). Wang et al. (Wang et al., 2021,2023) studied the deformation of the scroll under the action of temperature, pressure and inertial force through fluid-solid-thermal coupling. They found that thermal deformation caused by temperature is the most significant. The OS and the FS will come into contact during the movement, and the side and radial leakage gaps show spatiotemporal inhomogeneity. The wrap height can be adjusted using CFD/CSM, with the height gradually decreasing from the outer to the inner region to minimize radial leakage and improve compressor performance.

In most CFD models of air conditioning compressors, the flow domain is often simplified. However, in this paper, to investigate the suction and discharge pressure pulsations of electric vehicle air conditioning scroll compressors, we established a complete flow domain model. Through this model, we analyzed the unsteady process inside the scroll compressor, compared with the simplified model, and gave suggestions for model simplification. The suction and discharge pressure pulsations under different speeds and structures are analyzed, and examples are given.

2. Geometry and Methodology

2.1 Geometry

The structure of the electric scroll compressor is shown in Figure 1. The compressor is a horizontal, low back pressure refrigeration scroll compressor. The refrigerant gas enters the casing through the suction pipe, enters the orbiting scroll (OS) and fixed scroll (FS) after cooling the motor. The refrigerant gas passes through the crescent-shaped working chamber formed by the OS and FS, undergoing periodic suction and compression. Finally, it exits the compressor through the discharge valve into the exhaust chamber. The oil and gas mixture in the exhaust chamber is separated from the oil and gas through the cyclone separation structure of the exhaust pipe. In the exhaust chamber, a cyclone separation structure separates the oil and gas mixture, directing the separated lubricating oil into the oil pool while discharging the gas from the compressor. Both the OS and FS feature sealing strip grooves at their tops, allowing for axial clearance adjustment via the sealing strip. To ensure radial sealing and minimize

circumferential leakage, a radial flexible sealing mechanism is employed to adjust the radial gap between the two scrolls. Additionally, a cylindrical pin and ring structure prevent the rotation of the OS.

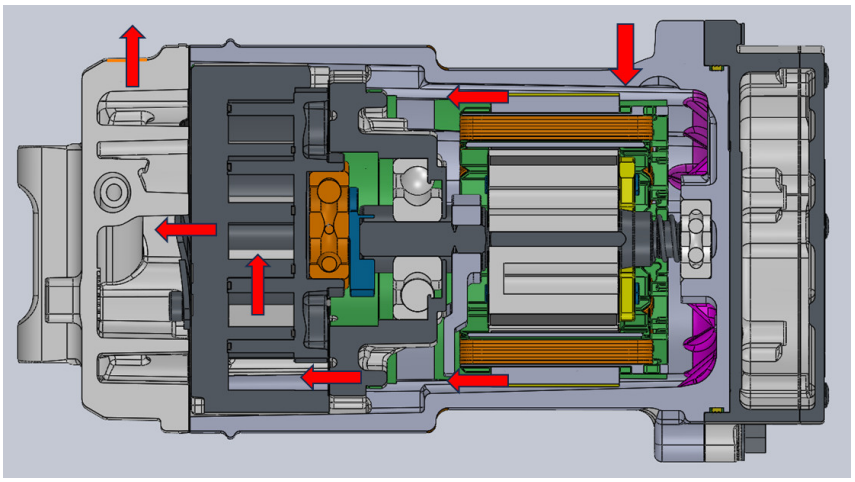

Figure 1: Electric scroll compressor structure

The FS and OS profiles utilize PMP profiles, as shown in Figure 2. The scroll wrap height is 21.8mm and the displacement is 45cc·min^{-1}.

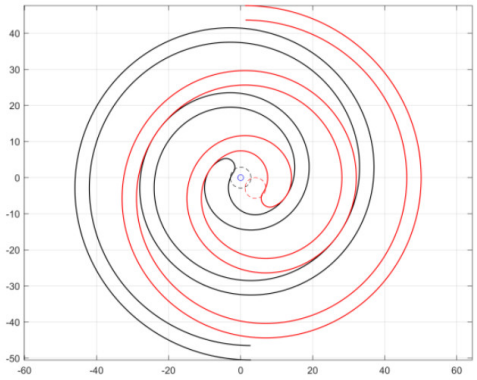

Figure 2: Electric scroll compressor structure

2.2 CFD Model

This article ignores the air gap between the motor rotor and stator, treating the motor as a solid cylinder. Additionally, it overlooks the small fluid domain around the bracket. Finally, the complete fluid domain for calculation is obtained. From the complete fluid domain, the partial fluid domain of the motor and the oil pool where lubricating oil accumulates at the exhaust are removed, and a simplified fluid domain is obtained.

The actual model is shown in Figure 3. The sky-blue fluid domain contains a rotating part comprising by FS and OS. Additionally, there is a crescent-shaped domain designed to prevent over-compression. The figure illustrates six parts of the domain, each interconnected through interfaces. Specific descriptions of each fluid domain are provided in Table 1.

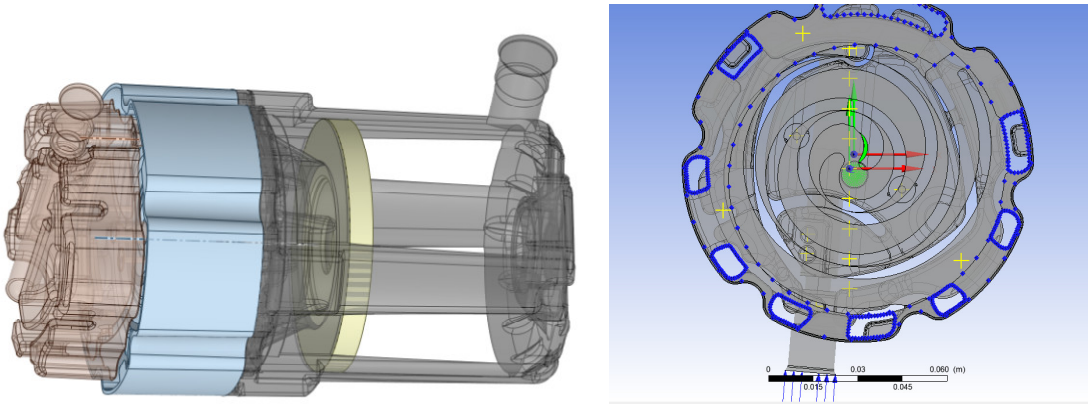

(a) Complete model (b) Simplified model

Figure 3: The fluid models

Table 1: Fluid domain properties and motion

Fluid domain color	Domian name	Properties	Motion
Gery	Suction Domain	Motor and bracket	Fixed
Yellow	Rotating Domian	Main balancing block	Rotating around the center of the FS (or motor shaft)
Blue	Connection Domain	Suction of the simplified model	Fixed
Brown	Discharge Domain	Exhaust chamber and oil-gas separator	Fixed
Green	Rotor Domian	Fixed and orbiting scroll	Rotor grid based on rotating angle
Red	Crescent Domain	Groove at beginning of the OS	Translation around the center of the FS base circle

The crescent-shaped fluid domain significantly impacts calculation accuracy. Its absence would lead to over-compression of up to 2MPa. Therefore, this article takes into account its existence during the analysis.

The CFD model adheres to principles of mass conservation and energy conservation, employing the SST k-ω turbulence model and the total energy model for analysis. Opening boundaries are applied to both the inlet and outlet. To address the valve's influence, this article employs the opening and closing conditions of the CFX software to simulate the valve's operation. The opening pressure difference of the valve is determined through experiment. When the pressure difference is approximately 0.18MPa, the valve is partially open, and at 0.3MPa, it is fully open. During the software setting process, the pressure difference for opening and closing is 0.15MPa. However, there remains a difference from the actual operating conditions.

2.3 Grid Independent

Due to the complex shape, the static part of the fluid domain can be divided into tetrahedral meshes to ensure the number of meshes with gaps. The rotating flow domain composed by FS and OS has complex deformations. To address this, this article employs the TwinMesh software developed by CFX Berlin to generate high-quality meshes. Using the 1° angle step and the grid size 1mm, the circumferential distribution of elements remains relatively uniform. Nonetheless, grid independence tests are essential in both the radial and axial directions under the 1mm grid size setting. The results of the grid independence tests are presented in Table 2. The accuracy of calculations is notably influenced by the number of axial grids. It is important to ensure that there is an axial boundary layer and that the grid size in the center is equivalent to a 1mm grid size. When the radial grid comprises approximately 18 layers or more, its effect on calculation results is negligible. Consequently, this paper adopts a grid generation configuration comprising 26 elements in the axial direction and 18 elements in the radial direction.

Table 2: Grid independence

Configuration	Radial elements	Axial elements	Mass flow rate/kg·s^{-1}	Error/%
No.1	14	18	0.0487	-7.33
No.2	14	22	0.0496	-5.61
No.3	14	26	0.0503	-4.28
No.4	16	22	0.0510	-2.95
No.5	16	26	0.0516	-1.81
No.6	18	22	0.0518	-1.43
No.7	18	26	0.0525	-0.095
No.8	20	22	0.0521	-0.86
No.9	20	26	0.0526	0.095

* The baseline value is the average of mass flow rates (configuration No.7 and No.9)

2.4 Experimental Validation

The compressor performance is tested using a standard electric scroll compressor performance test bench. This paper tests the compressor performance of the scroll compressor at different speeds under the conditions of an inlet pressure of 3 bar and an outlet pressure of 15 bar. The compressor and system performance data at different speeds are shown in Table 3. The simulation results are in good agreement with the experimental results, as shown in Figure 4. The simulation errors are mainly caused by thermal deformation of the scroll, valve opening pressure difference, and suction heating of the motor. In addition, all the CFD model does not take into account the effect of lubricating oil.

Table 3: Experimental data

Rotating speed/rpm	Cooling capacity/kW	Input power/kW	Discharge temperature/℃	Mass flow rate/kg·h^{-1}	Volumetric efficiency/%
3000	4.0276	1.69	81.66	104.64	92.7
4000	5.4582	2.27	80.53	143	94.1
5000	6.8797	2.87	83.92	179.59	94.6
6000	8.198	3.55	82.5	216.39	95.3
7000	9.576	4.28	84.18	252	95.2
8000	10.8805	5.06	85.38	286.53	94.3
9000	12.0144	5.86	87.95	318.15	93.1
10000	13.2427	6.76	90.23	349.35	91.9
11000	14.2447	7.71	93.63	376.8	90.3

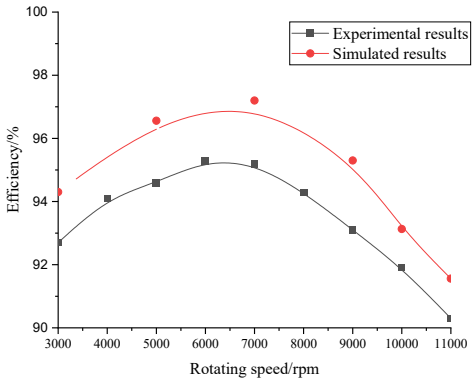

Figure 4: Simulated results compared with experimental data

3. Result and Discussion

3.1 Complete Model Performance

The mass flow and efficiency of the complete model are shown in Figure 5. At speeds of 5,000 rpm and 10,000 rpm, the inlet and outlet mass flow errors are both under 5%, indicating model convergence. As the speed increases from 5000rpm to 10000rpm, the volumetric efficiency decreases by 3.43%, and the isentropic efficiency decreases by 1.91%. As the rotating speed increases, the volumetric efficiency increases first and then decreases, and the simulation and experimental trends are consistent.

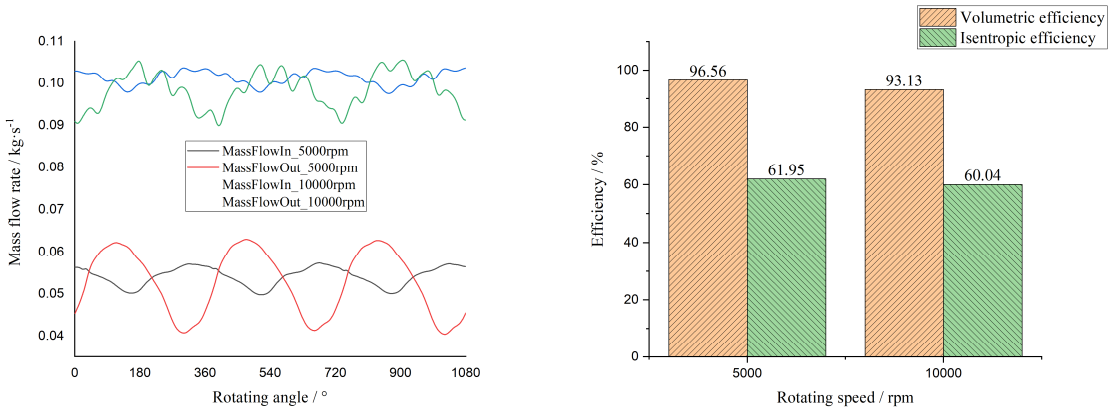

(a) Mass flow rate (b) Efficiency

Figure 5: Mass flow rate and efficiency of the complete model

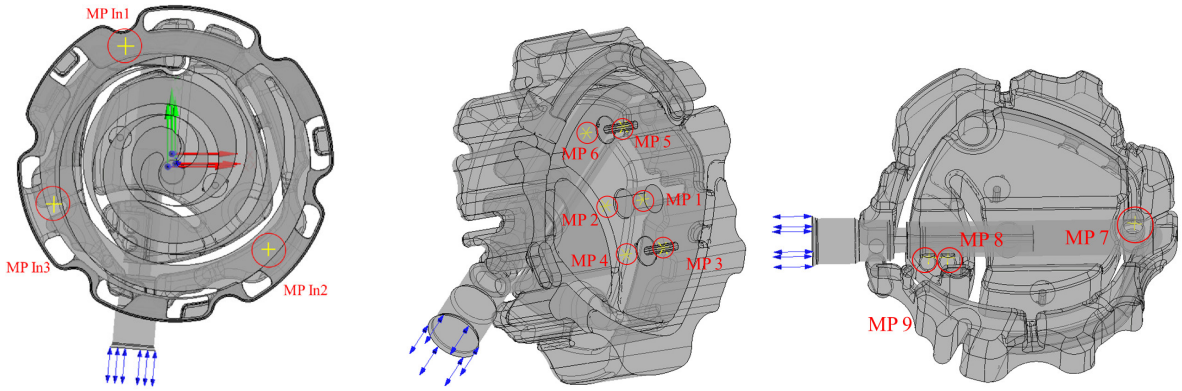

Figure 6: The location of the inlet pressure monitoring point and its fluctuations

To investigate the pressure loss and pressure pulsation of the suction and exhaust, three and six monitoring points were respectively established. The location of the monitoring points is shown in Figure 6. It's important to note that for the monitored points 3 and 5, corresponding to the pressures of the pressure relief holes, all pressure relief valves were closed during the working conditions calculated in this study.

At 5000rpm, the motor cavity domain causes an average pressure loss of about 10000Pa, and when the rotational speed is increased to 10000rpm, the pressure loss increases to 37500Pa. Similarly, the pressure loss caused by the exhaust buffer chamber and separation structure increased from 80000Pa to 240000Pa. Therefore, when calculating high-speed operating conditions, the pressure loss at the exhaust should be considered. The pressure of the complete model within one cycle was shown in Figure 8.

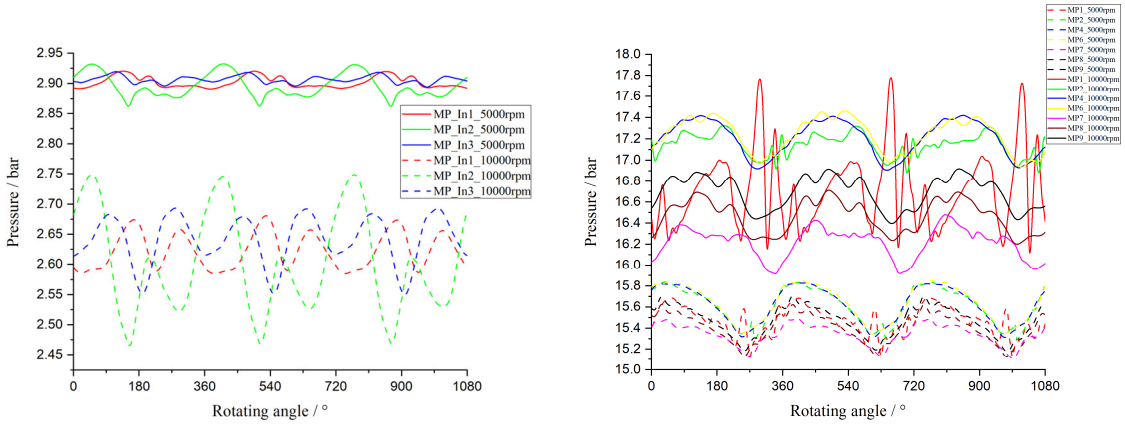

(a) Suction side (b) Discharge side

Figure 7: The location of the discharge part monitoring point

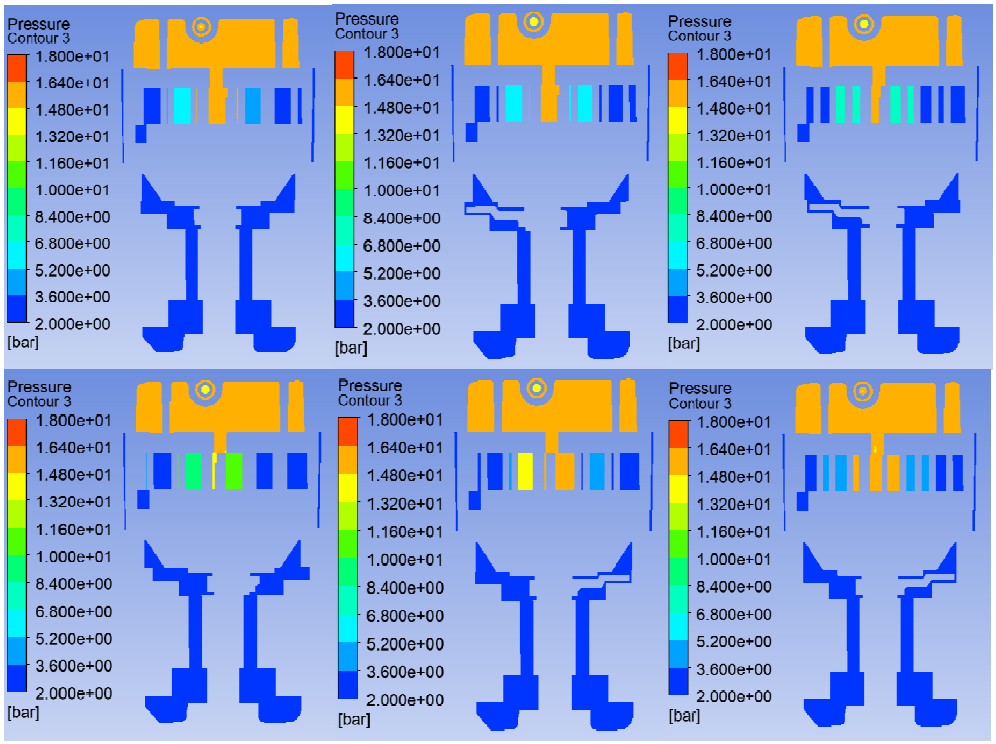

Figure 8: The pressure of the complete model within one cycle

3.2 Simplified Model Performance

The performance of the simplified model at 5900rpm, 8600rpm and 11000rpm is shown in Figure 9. The mass flow rate at the inlet and outlet fluctuates continuously within three cycles, and the error is less than 5%. As the rotational speed increases, both the volumetric efficiency and the isentropic efficiency initially decrease and then increase. The volumetric efficiency and isentropic efficiency of the simplified model are both greater than that of the complete model. This is due to the fact that the simplified model does not consider the motor cavity domain and the inlet area is greatly different. The inlet area of the simplified model is 6.3 times that of the compressor inlet area of the complete model.

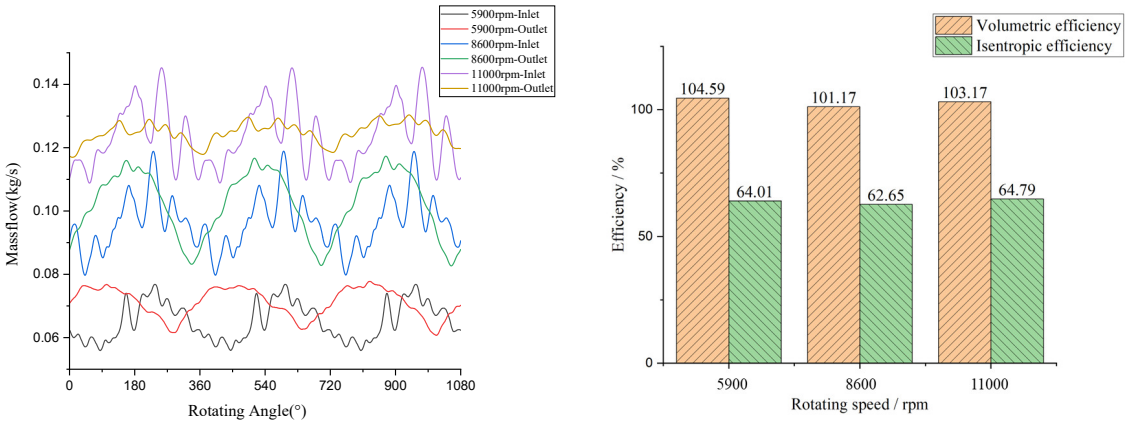

(a) Mass flow rate (b) Efficiency

Figure 9: Mass flow rate and efficiency of the simplified model

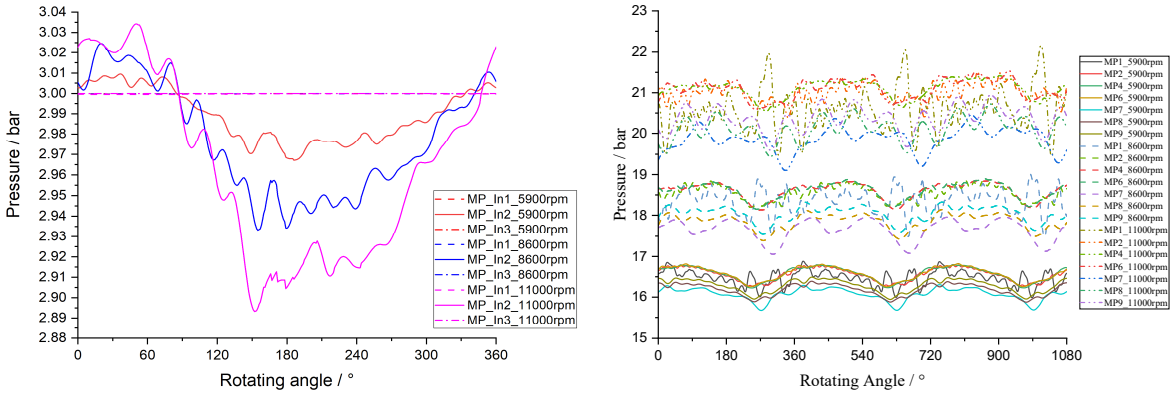

(a) Suction side (b) Discharge side

Figure 10: The pressure pulsation under different speeds of the simplified model

The pressure pulsations at the suction and exhaust were also monitored in Figure10. The suction pressure pulsation is significantly reduced, with the maximum fluctuation reaching only 10000 Pa at 11000 rpm. However, the pulsation of the exhaust showed a general increase. At rotating speed of 5900rpm, 8600rpm and 11000rpm, the pressure loss is 180000Pa, 380000Pa and 600000Pa respectively. This particularly large pressure loss may be due to the lack of buffering in the motor cavity domain and the excessive gas inlet area.

3.3 Pulsation Analysis and Improvement

The pressure coefficient C_p is used to describe the pressure pulsation, P_{ave} is the average pressure within a period, and ΔP is the difference between the pressure and the P_{ave}.

$$C_p = \Delta P / P_{ave} \tag{1}$$

After decomposing the pressure fluctuation in both the time domain and frequency domain, the frequency values affecting the pressure fluctuation can be determined. The frequency domain diagram of the suction and exhaust pressure coefficient C_p at 5900 rpm is shown in Figure 11. At a rotational speed of 5900rpm, the rotation frequency is 98.33Hz, with the main frequency recorded at 98.06Hz. Notably, the main frequency is 0.997 times the rotation frequency. This phenomenon is consistent across other rotational speeds as well.

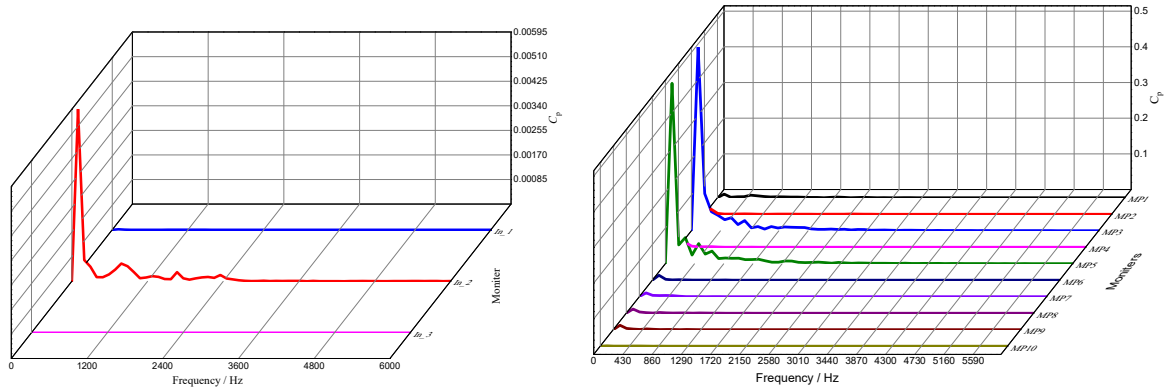

(a) Suction side (b) Discharge side

Figure 11: The pressure pulsation under different speeds of the simplified model

To reduce the pressure pulsation and noise in the exhaust, the original structure of the FS and OS was optimized. The old model and the new model were shown in Figure 12. The diameter of the exhaust hole is changed from 8.7mm to 9.7mm. While the depth of the crescent groove remains unchanged, the area has been changed from 10.69 mm² to 33.48 mm².

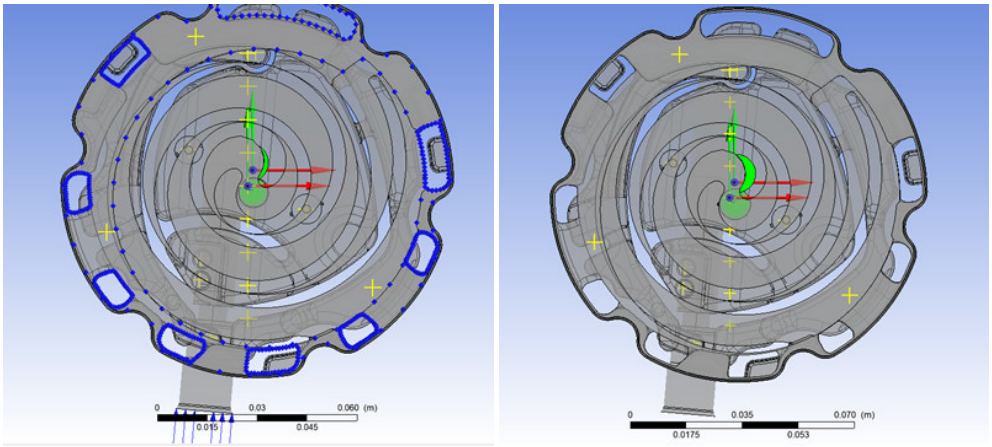

(a) The old model (b) The new model

Figure 12: The old model and the new model of OS and FS

The performance comparison before and after the improvement is shown in Figures 13 and 14. The fluctuation of the central compression chamber is reduced, and the over-compression is reduced from 17.9bar to 17.6bar. Additionally, the pressure of the two symmetrical second compression chambers exhibit a more consistent upward trend. However, the theoretical gas power has increased by 58.76W compared to before optimization. Furthermore, the noise of the two structures was tested through experiments. The optimized structure noise was reduced by 3.2dBA compared with the previous structure.

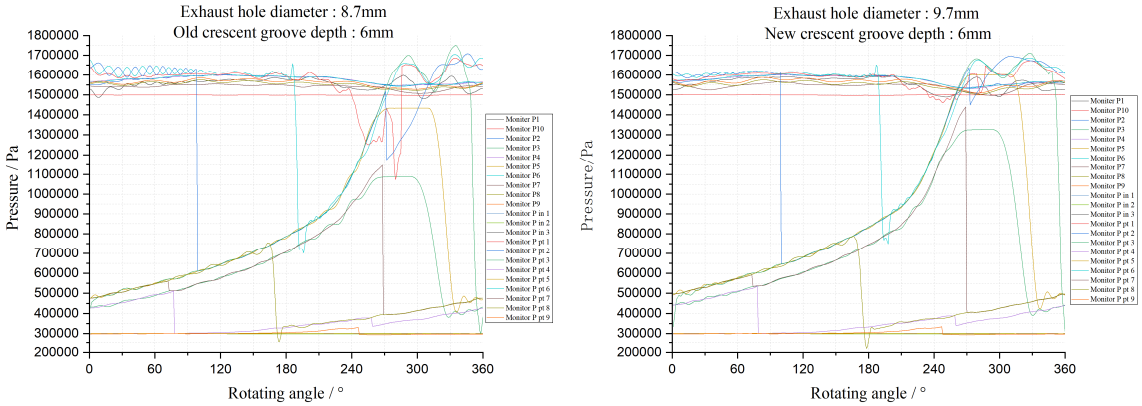

(a) The old model (b) The new model

Figure 13: The pressure changes between the old and new models

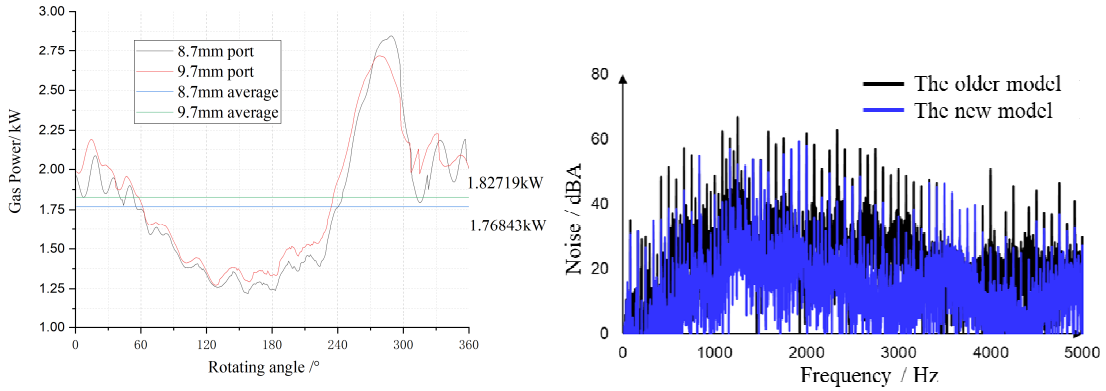

(a) The power comparison (b) The noise comparison

Figure 14: The changes in gas power and noise between old and new models

6. CONCLUSIONS

The conclusions of this article are as follows:

- To account for the motor cavity domain and main balance blocking domain, a complete fluid domain model for an electric scroll compressor was established.
- Comparing the complete model and the simplified model, it was found that the suction and exhaust pressure loss should be considered in model simplification. In addition, the suction area can also be equivalently simplified to prevent errors caused by excessive non-actual suction area.
- Enlarging the exhaust port diameter and crescent groove area can effectively reduce over-compression in the central compression chamber and noise levels. However, increasing the area may lead to heightened leakage from the central chamber to the second compression chamber. It's crucial to prevent the relief valve from opening in such situations.

REFERENCES

Bin, P., Lemort, V., Legros, A., Hongsheng, Z., & Haifeng, G. (2017). Variable thickness scroll compressor performance analysis—Part I: Geometric and thermodynamic modeling. *Proceedings of the Institution of Mechanical Engineers, Part E: Journal of Process Mechanical Engineering*, *231*(4), 633-640.

Bin, P., Lemort, V., Legros, A., Hongsheng, Z., & Haifeng, G. (2017). Variable thickness scroll compressor performance analysis—Part II: Dynamic modeling and model validation. *Proceedings of the Institution of Mechanical Engineers, Part E: Journal of Process Mechanical Engineering*, *231*(4), 641-649.

Cavazzini, G., Giacomel, F., Benato, A., Nascimben, F., & Ardizzon, G. (2021). Analysis of the inner fluid-dynamics of scroll compressors and comparison between CFD numerical and modelling approaches. *Energies*, *14*(4), 1158.

Ding, J., Yue, X., Zhang, Y., Yang, F., Cao, H., & Ba, D. (2022). Analysis of the transient flow in a scroll-type compressor constructed from an algebraic spiral with pressure relief valves. *Journal of the Brazilian Society of Mechanical Sciences and Engineering*, *44*(8), 379.

Li, X., Wu, W., Zhang, J., Guo, C., Ke, F., & Jiang, F. (2023). Analysis of 3D transient flow in a high-speed scroll refrigeration compressor. *Energies*, *16*(7), 3089.

Sun, S., Wu, K., Guo, P., & Yan, J. (2017). Analysis of the three-dimensional transient flow in a scroll refrigeration compressor. *Applied Thermal Engineering*, *127*, 1086-1094.

Sun, S., Wang, Z., Guo, P., & Mao, Z. (2021). Optimization of the tip profile of orbiting scroll in an asymmetry suction chamber scroll compressor. In *IOP Conference Series: Materials Science and Engineering* (Vol. 1180, No. 1, p. 012014). IOP Publishing.

Sun, S., Wang, X., Guo, P., Zheng, X., & Yan, J. (2019). Optimization of suction chamber structure in a scroll refrigeration compressor. In *IOP Conference Series: Materials Science and Engineerin*g (Vol. 604, No. 1, p. 012080). IOP Publishing.

TAKASU, Y., KIMATA, Y., HOTTA, Y., SATO, H., ITO, T., & YAMASHITA, T. (2019). Development of Evolutionary Three-Dimensional Scroll Compressor Realizes Energy Saving in Air Conditioning and Refrigeration Equipment. *Mitsubishi Heavy Industries Technical Review*, *56*(4), 1-6.

Wang, C., Zhang, S., Zhao, Z., Cheng, J., & Wu, J. (2023). Study on the contact and size of radial and flank leakage gaps of scrolls in a scroll compressor with CFD/CSM simulations. *International Journal of Refrigeration*, *149*, 73-82.

Wang, C., Zhang, S., Cheng, J. M., Lei, B. W., Du, Y. J., & Wu, J. H. (2021, September). Simulation of the Deformation and Contact of Scrolls in the Scroll Compressor. In *IOP Conference Series: Materials Science and Engineering* (Vol. 1180, No. 1, p. 012013). IOP Publishing.

Zhang, S., Wu, J., Wang, C., Zhong, H., & Zhao, Z. (2023). Study on a variable wall thickness profile of electric scroll compressor used for automobile air conditioner. *Proceedings of the Institution of Mechanical Engineers, Part A: Journal of Power and Energy*, *237*(2), 294-307.

Zhang, X., Zhang, B., Cao, J., Su, L., & Li, K. (2022). Numerical investigation on the performance and vapor injection process of a scroll compressor with different injection features. *Applied Thermal Engineering*, *217*, 119061.

Zhang, Y., Peng, B., Zhang, P., Sun, J., & Liao, Z. (2024). Key Technologies and Application of Electric Scroll Compressors: A Review. *Energies*, *17*(7), 1790.

ACKNOWLEDGEMENT

We are very grateful to Suzhou Zhongcheng New Energy Technology Co., Ltd. for its help in experimental testing.